Sensors & Transducers, Vol. 169, Issue 4, April 2014, pp. 9-17

Sensors & Transducers

Speed Sensorless Control of Permanent Magnet Synchronous Motors in Mine Electric Locomotive Drive

[1] Yudong LI, [1] Xiaobang YANG and [2] Tianyu ZHANG
[1] School of Electrical Engineering & Automation Henan Polytechnic University (HPU), P. R. China
[2] School of Mechanical and Electrical Engineering, Henan Vocational College of Industry and Information Technology, 801 Bilian Avenue, Jiaozuo, Henan, 454000, P. R. China
[1] Tel.: 0391-3987592, fax: 0391-3987596
E-mail: lyd@hpu.edu.cn

Received: 23 January 2014 /Accepted: 7 March 2014 /Published: 30 April 2014

Abstract: This paper presents a novel sensorless control method of permanent magnet synchronous motors a low speed based on a high-frequency voltage signal injection. The approach superimposes a persistent HF voltage signal into the estimated d-axis to get the rotor position error angle-related signal by detecting the corresponding voltage response and current response. Then the rotor position and motor speed are obtained. Theoretical analysis and simulation results demonstrate that the approach can achieve sensorless control of permanent magnet synchronous motors at zero and low speed, ensure good dynamic and static performances, and achieve effective control when applied to servo system. Finally, a test prototype system which used a digital signal processor and space vector pulse width modulation technology has been developed. Experimental results show that the system has better static, the effectiveness and dynamic performance of the adaptive test signals in a sensorless controlled surface-mounted permanent magnet synchronous machines.

Keywords: Direct-current line electric locomotive, Variable frequency drive, Voltage signal injection, Permanent magnet synchronous machine (PMSM).

1. Introduction

Mining electric locomotive is one of the electrical equipments of traction, most electric locomotives driven by direct-current (DC) motor, and its speed controlled by series connection resistances. The DC drives have complex structure, low efficiency, maintenance of large, short life and other issue [1-3]. Today PMSM drives are gradually replacing classic DC drives in a large number of industrial applications, taking full advantage of key features of PM-motors, such as compactness, robustness, high efficiency, reliability and shape adaptation to the working environment [2-6]. However, to achieve precisely control of PMSM, rotor position and speed are needed. Thus mechanical position sensors are usually installed, resulting in an increasing of the cost, size and maintenance difficulties. The sensorless vector control of PMSM has been under keen research for decades [1-3].

Various sensorless control schemes have been presented by scholars. Generally, according to the estimated effect at different speed ranges, sensorless control methods can be classified into two main types [10-12]: one is to zero and low speed, and the other is applicable to medium and high speed. The former is mostly based on high frequency model of motor. Using the non-ideal characteristics of PMSM

structure or inductor saturation effect, a high-frequency (HF) signal is superimposed on the stator voltage or stator current and rotor position information can be received from the corresponding current component [7-12]. These methods pose various advantages such as insusceptibility to electrical parameter variations, good robustness and superiority of position estimation at zero and low speed. Typically, the injected signal can be a rotating HF voltage vector, a rotating HF current vector or a pulsating HF voltage vector. As a consequence, most of them are more suitable for interior permanent magnet synchronous motors (IPMSM), which has inherent saliency. The pulsating HF voltage injection is carried out by the application of a HF sinusoidal voltage signal along the estimated synchronous reference frame, taking advantage of the saliency caused by inductor saturation [11, 12].

In [8-10], LF current signal is injected to the stator current and the resulting response of back-electromotive force (EMF) is used to estimate the rotor speed. This method doesn't rely on the rotor saliency but just the fundamental-wave model, so it's very suitable for surface-mounted permanent magnet synchronous machines (SPMSM).

The paper presents a novel sensorless control method based on the superimposition of a HF voltage vector along the estimated PMSM model d-axis. The approach superimposes a persistent LF voltage signal into the estimated d-axis to get the rotor position error angle-related signal by detecting the corresponding voltage response and current response. Then the rotor position is obtained. Theoretical analysis and simulation results demonstrate that the approach can achieve sensorless control of PMSM at zero and low speed, ensure good dynamic and static performances, and achieve effective control when applied to servo system. Finally, a test prototype system has been developed. The system device replaces the series resistance, greatly reduces the size of the control system, and realizes the integration. Currently, the system device has been applied to direct-current lines of the coal mine electric locomotive.

2. The Mathematic Model of PMSM

For simplicity, several assumptions are made in the SPMSM mathematical model. The magnetic field is spatially sinusoidal and eddy current and hysteresis losses are assumed to be negligible. Then id = 0 rotor magnetic field oriented control strategy is adopted. The electrical equations of the PMSM can be described in the d-q rotating reference frame as follows:

$$\begin{bmatrix} u_d \\ u_q \end{bmatrix} = \begin{bmatrix} R_s & -\omega L_q \\ \omega L_d & R_s \end{bmatrix} \begin{bmatrix} i_d \\ i_q \end{bmatrix} + \begin{bmatrix} L_d & 0 \\ 0 & L_q \end{bmatrix} p \begin{bmatrix} i_d \\ i_q \end{bmatrix} + \begin{bmatrix} 0 \\ \omega\psi_f \end{bmatrix}, \quad (1)$$

where L_d, L_q, u_d, u_q, i_d, i_q are the d, q frame inductances, stator voltages and currents respectively; ψ_f is the rotor flux; R_s is the stator resistance; ω is the electrical angular speed and p is the differential operator.

The cross coupling terms and back-EMF of (1) can be negligible at zero and low speed. Thus, (1) is simplified:

$$\begin{bmatrix} u_d \\ u_q \end{bmatrix} = \begin{bmatrix} R_s & 0 \\ 0 & R_s \end{bmatrix} \begin{bmatrix} i_d \\ i_q \end{bmatrix} + \begin{bmatrix} L_d & 0 \\ 0 & L_q \end{bmatrix} p \begin{bmatrix} i_d \\ i_q \end{bmatrix} = \begin{bmatrix} Z_d & 0 \\ 0 & Z_q \end{bmatrix} \begin{bmatrix} i_d \\ i_q \end{bmatrix}, \quad (2)$$

where Z_d, Z_q are the d, q frame impedances respectively.

3. Abbreviations and Acronyms

3.1. SPMSM Inductor Saturation Effect

Since the magnetic permeability of SPMSM permanent magnet is approximately equal to that of the air gap, it is normally considered that d, q frame inductances are equal; but the magnetic saturation will lower the d-axis inductance. Therefore, SPMSM shows "small saliency", that is, in other words, inductor saturation effect [11, 12].

The air gap magnetic field of SPMSM is composed of permanent magnet and stator current magnetic field. The rotor magnet can be equivalent to the magnetic field excitation current if. The curve of d-axis magnetic circuit characteristic can be approximately shown as Fig. 1 (a). The operating point of d-axis magnetic circuit is decided by if, shown as point A. With a certain positive current injected, the d-axis magnetic field will be saturated; on the contrary, a negative current makes the magnetic circuit work in the linear region. Defining L_d^+ as d-axis positive inductance and L_d^- as negative inductance, the following relation can be obtained: $L_d^+ < L_d < L_d^-$.

The curve of q-axis magnetic circuit is basically the same as that of d-axis. The operating point is at the origin, and the magnetic circuit works in the linear region without saturation. Similarly, define L_d^+ as d-axis positive inductance and L_d^- as negative inductance, then $L_q^+ = L_q^- = L_q$.

Since the curves are basically same, it can be considered $L_q \approx L_d^-$, thus $L_d < L_q$.

3.2. The Principle of Sensorless Control at Low Speed

The estimated error angle $\Delta\theta$ is defined as follows [13, 14]:

$$\Delta\theta = \theta - \hat{\theta}, \quad (3)$$

The relationship among actual position angleθ, estimated position angle $\hat{\theta}$ and estimated error angle Δθ is shown in Fig. 1(b).

When the motor is in low or zero speed and back EMF can be negligible, voltage equations are simplified as:

$$\begin{bmatrix} u_d \\ u_q \end{bmatrix} = \begin{bmatrix} r + L_d p & 0 \\ 0 & r + L_q p \end{bmatrix} \begin{bmatrix} i_d \\ i_q \end{bmatrix}, \quad (4)$$

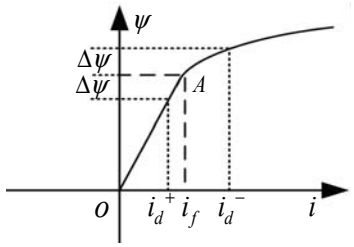

(a) The curve of d-axis magnetic characteristic.

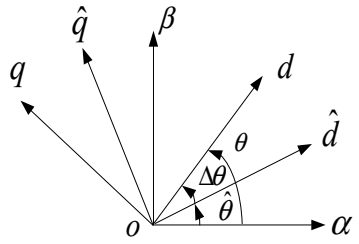

(b) The diagram of coordinate systems.

Fig. 1. The Principle of Sensorless Control.

The equivalent circuit of PMSM in the two-phase rotating coordinate system is shown in Fig. 2.

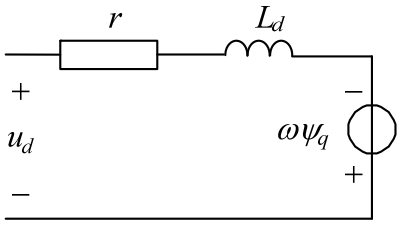

(a) Equivalent circuits of d-axis.

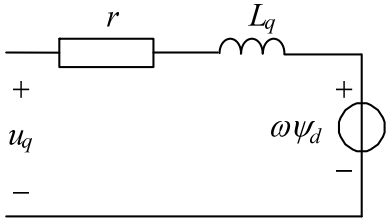

(b) Equivalent circuits of q-axis.

Fig. 2. The equivalent circuit of PMSM in the two-phase rotating coordinate system.

When a fluctuating high frequency voltage is injected in the two-phase rotating coordinate system, (4) can be expressed in impedance form as follows:

$$\begin{bmatrix} u_{dh} \\ u_{qh} \end{bmatrix} = \begin{bmatrix} Z_d & 0 \\ 0 & Z_q \end{bmatrix} \begin{bmatrix} i_{dh} \\ i_{qh} \end{bmatrix}, \quad (5)$$

In Fig. 1(b), the relationship of two voltages in the two coordinate systems as follows:

$$\begin{bmatrix} u_d \\ u_q \end{bmatrix} = \begin{bmatrix} \cos\Delta\theta & \sin\Delta\theta \\ -\sin\Delta\theta & \cos\Delta\theta \end{bmatrix} \begin{bmatrix} \hat{u}_d \\ \hat{u}_q \end{bmatrix}, \quad (6)$$

$$\begin{bmatrix} i_d \\ i_q \end{bmatrix} = \begin{bmatrix} \cos\Delta\theta & \sin\Delta\theta \\ -\sin\Delta\theta & \cos\Delta\theta \end{bmatrix} \begin{bmatrix} \hat{i}_d \\ \hat{i}_q \end{bmatrix}, \quad (7)$$

Combining (5), (6) and (7), the following relationship can be deduced:

$$\begin{bmatrix} \hat{i}_{dh} \\ \hat{i}_{qh} \end{bmatrix} = \frac{1}{Z_d Z_q} \begin{bmatrix} Z - \Delta Z\cos(2\Delta\theta) & -\Delta Z\sin(2\Delta\theta) \\ -\Delta Z\sin(2\Delta\theta) & Z + \Delta Z\cos(2\Delta\theta) \end{bmatrix} \begin{bmatrix} \hat{u}_{dh} \\ \hat{u}_{qh} \end{bmatrix}, \quad (8)$$

where $Z=(Z_d+Z_q)/2$, $\Delta Z=(Z_d-Z_q)/2$.

From (8), it can be seen that both $\hat{i}_d$ and $\hat{i}_q$ have the components relative toΔθ. In order to accurately and easily extractΔθ, the HF voltage signal:

$$\begin{bmatrix} \hat{u}_{dh} \\ \hat{u}_{qh} \end{bmatrix} = \begin{bmatrix} U_{\mathrm{m}} \cos\omega_{\mathrm{h}} t \\ 0 \end{bmatrix}, \quad (9)$$

the HF voltage signal (9) can be injected into $\hat{d} - \hat{q}$ frame, where Um is the amplitude of the voltage signal, and ω_h is the angular frequency. Thus, the HF voltage response in the $\hat{d} - \hat{q}$ frame is:

$$\begin{bmatrix} \hat{i}_{dh} \\ \hat{i}_{qh} \end{bmatrix} = \begin{bmatrix} \dfrac{Z - \Delta Z\cos(2\Delta\theta)}{Z_d Z_q} U_{\mathrm{m}} \cos\omega_{\mathrm{h}} t \\ \dfrac{-\Delta Z\sin(2\Delta\theta)}{Z_d Z_q} U_{\mathrm{m}} \cos\omega_{\mathrm{h}} t \end{bmatrix}, \quad (10)$$

Under a high-frequency excitation, the d, q-axis impedance satisfies the following formula:

$$Z_d = r + j\omega_h L_d = |Z_d| \angle\varphi_d, \quad (11)$$

$$Z_q = r + j\omega_h L_q = |Z_q| \angle\varphi_q, \quad (12)$$

Combining (8), (9) and (10), $\hat{i}_{qh}$ can be deduced:

$$\hat{i}_{qh} = \frac{\omega_{\mathrm{h}} \Delta L U_{\mathrm{m}}}{|Z_d||Z_q|} \sin(2\Delta\theta)\sin(\omega_{\mathrm{h}} t - \varphi_d - \varphi_q) \quad (13)$$

When $\Delta\theta \to 0$, $i_{qh} = \hat{i}_{qh} = 0$, the injected HF signal will not produce torque ripples, ensuring good performance of the method.

First of all, the amplitude of $\hat{i}_{qh}$ will be modulated as follows:

$$\begin{aligned} f_{\Delta\theta} &= LPF(\hat{i}_{qh} \times \sin \omega_h t) \\ &= \frac{\omega_h \Delta L U_m \cos(\varphi_d + \varphi_q)}{2 \mid Z_d \mid\mid Z_q \mid} \sin 2\Delta\theta \,, \\ &= k \sin 2\Delta\theta \end{aligned} \tag{14}$$

where $k = \dfrac{\omega_h \Delta L U_m \cos(\varphi_d + \varphi_q)}{2 \mid Z_d \mid\mid Z_q \mid}$.

From (8), when $\Delta\theta \to 0$, $f\Delta\theta = 0$. If $f\Delta\theta$ will be regulated to zero, position $\hat{\theta}$ can be estimated. The structure diagram of regulation system and the signal processing are established as Fig. 3 and Fig. 4. Regulated by a PI regulator until $f\Delta\theta$ tends to 0, the output of the PI regulator and integrator is the estimated rotor position $\hat{\omega}$ and $\hat{\theta}$.

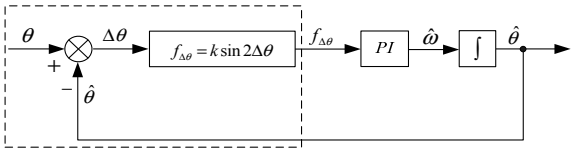

Fig. 3. The structure diagram of regulation system.

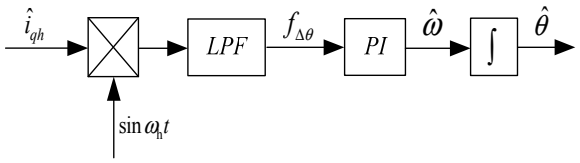

Fig. 4. The signal processing.

3.3. The Initial Rotor Position Estimation of Sensorless Control

The (-π/2,3π/2) electrical angle is divided into four intervals (0,π/2), (π/2,π), (π,3π/2) and (-π/2,0). If the initial value of $\hat{\theta}$ is zero, the convergence characteristics of Δθ can be drawn as follows in Table 1.

From the Table 1, it can be seen that there are two cases the convergence value of $\hat{\theta}$:

(a) If the convergence value of $\hat{\theta}$ is zero, the value of θ can be zero, π/2, π or 3π/2;

(b) If the convergence value of $\hat{\theta}$ is not zero, the value of θ can be $\hat{\theta}$ or $\hat{\theta}$+π.

From the above analysis, the following conclusions can be drawn. The actual position θ may be $\hat{\theta}$ or $\hat{\theta}$+π, that is to say, d-axis may be positive direction, also be a negative direction. Therefore the d-axis positive direction first must be determined in order to obtain the actual position of the rotor.

Table 1. The convergence characteristics of Δθ.

Actual θ	Δθ ($\hat{\theta}$=0)	Convergence value of Δθ	Convergence value of $\hat{\theta}$
(0,π/2)	(0,π/2)	0	θ
(π/2,π)	(π/2,π)	π	θ -π
(π,3π/2)	(π,3π/2)	π	θ -π
(-π/2,0)	(-π/2,0)	0	θ
0	0	0	0
π/2	π/2	π/2	0
π	π	π	0
3π/2	3π/2	3π/2	0

4. The system Simulation and Modeling

Fig. 3 shows the block diagram of SPMSM sensorless speed control system based on HF voltage signal injection, with a double-loop control structure. The inner loop is current loop for rotor position estimation and current regulation and the outer one is speed loop.

During the simulation of HF voltage injection sensorless speed control, switching frequency of the inverter is 10 kHz. A 1000 Hz voltage signal is injected, with the amplitude of 1 V. Simulation under a sudden change of speed command in 5s has been carried out, with the 1.0 rad, 2.1 rad, 4.7 rad, and 5.5 rad initial position and a transient speed command from 0 rpm to 60 rpm.

The initial position estimation procedure of the system runs in two phases. One is initial rotor position estimation in 2 seconds, the other is special position judgment and initial position correction during 2~3 seconds. The motor starts at 4.5 seconds, and the motor speed is increasing from 0 rpm to 60 rpm.

The simulation waveforms are shown in Fig. 5, Fig. 6, Fig. 7 and Fig. 8. In these figures, (a) is $\hat{\theta}$ and θ waveforms and (b) is Position estimation error $\Delta\theta$.

Simulation results indicate the effectiveness of the position estimation during start-up, constant speed and speed variation operation periods.

From Fig. 5 and Fig. 6 $\Delta\theta$ directly converges to 0 and don't need to be corrected. The control system is in a steady state. But from Fig. 7 and Fig. 8 $\Delta\theta$ don't directly converge to 0 and need to be corrected. Simulation results are consistent with the theoretical analysis. It is verified that the sensorless control method proposed is correct.

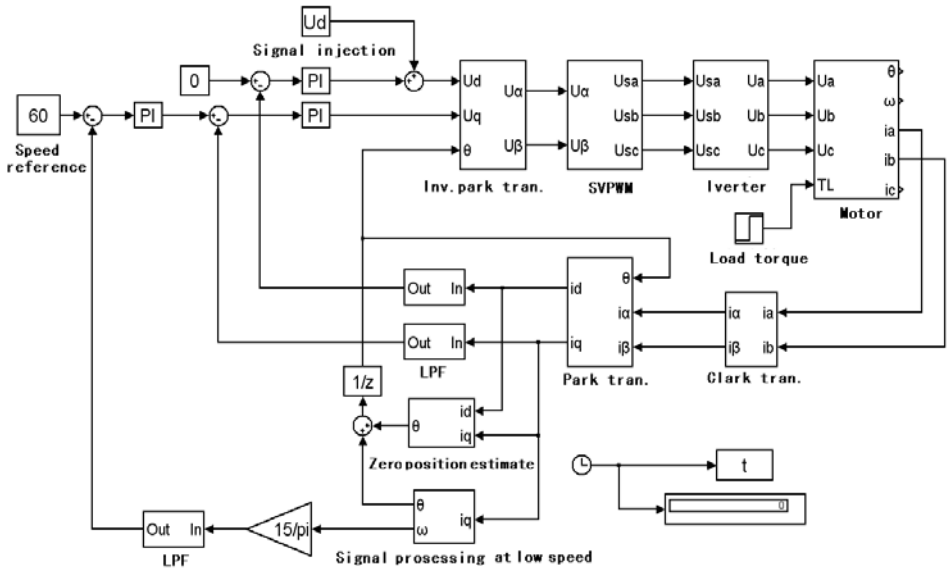

Fig. 3. The block diagram of SPMSM sensorless control at low speed.

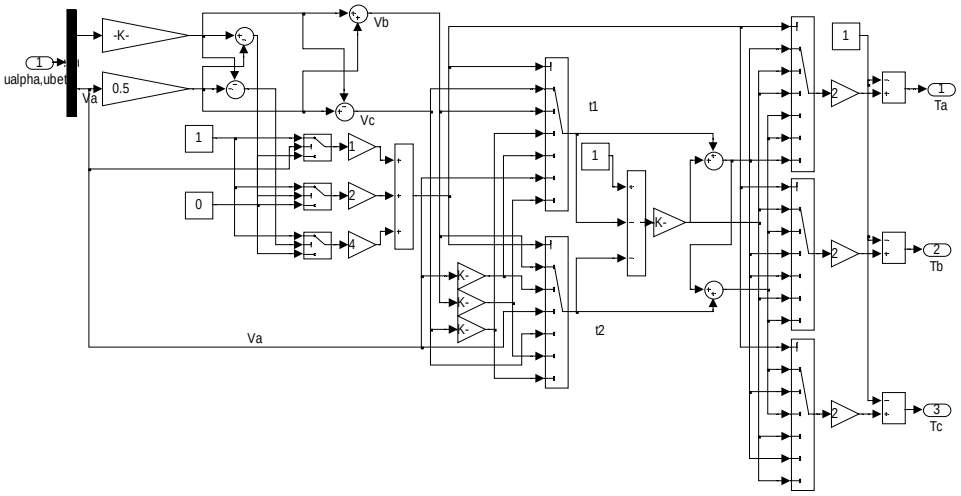

(a) Switching time calculation module.

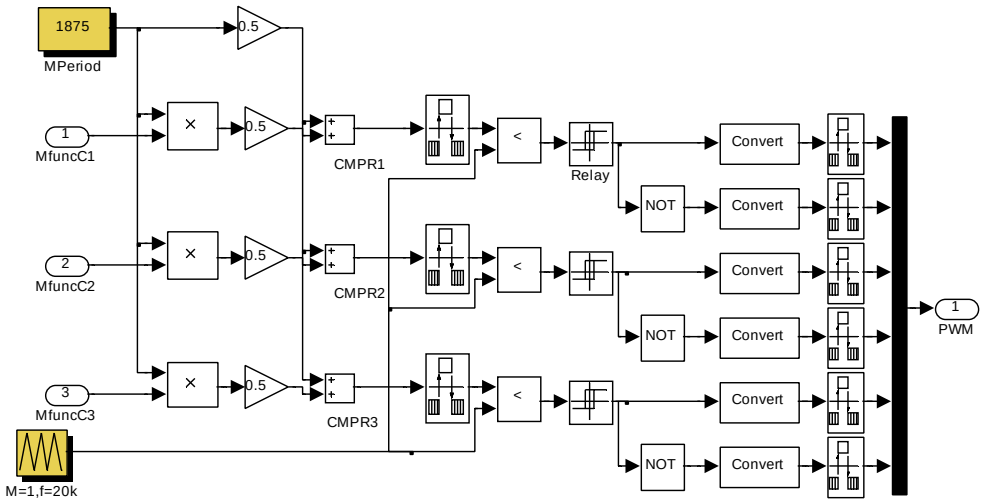

(b) Switching time calculation module.

Fig. 4. Space vector PWM wave generation modulation.

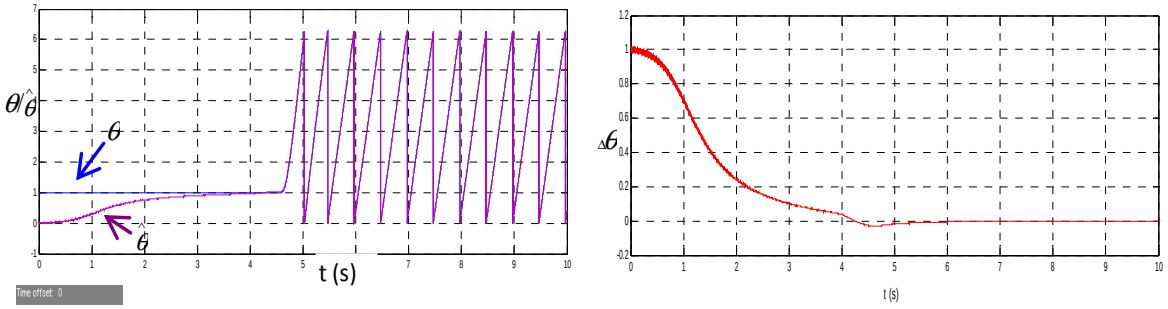

(a) Under the 1.0 rad initial position. (b) Under the 1.0 rad initial position.

Fig. 5. The estimated position and actual position waveforms simulated with 0 rpm speed command.

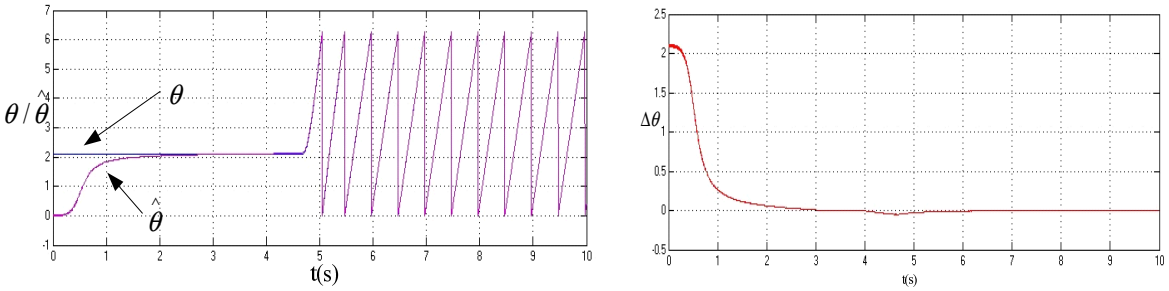

(a) Under the 2.1 rad initial position. (b) Under the 2.1 rad initial position.

Fig. 6. The estimated position and actual position waveforms simulated with 0 rpm speed command.

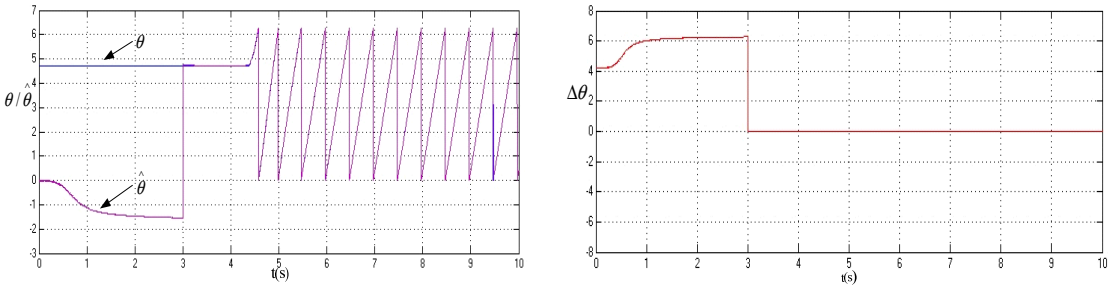

(a) Under the 4.7 rad initial position. (b) Under the 4.7 rad initial position.

Fig. 7. The estimated position and actual position waveforms simulated with 0 rpm speed command.

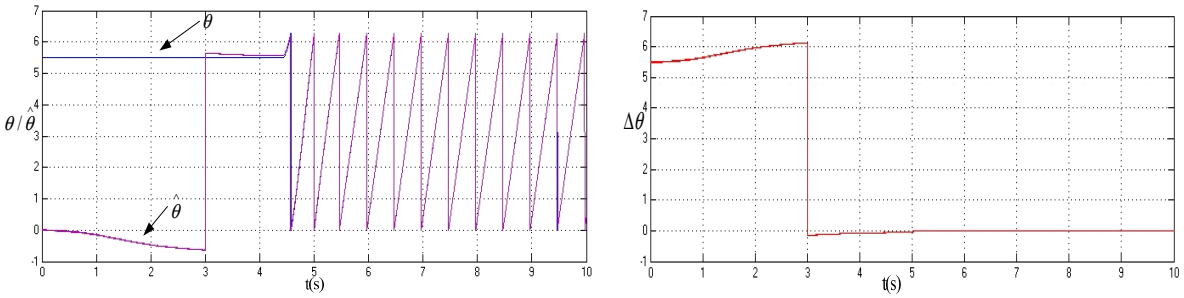

(a) Under the 5.5 rad initial position. (b) Under the 5.5 rad initial position.

Fig. 8. The estimated position and actual position waveforms simulated with 0 rpm speed command.

5. The System Design

5.1. Hardware Systems Design

System hardware circuit is drawn as Fig. 9. In order to reduce the electromagnetic interference, the control system hardware includes the DSP controller, the power converter, the regulate circuit, the keyboard display circuit and the auxiliary power supply circuit.

5.2. Software System Design

DSP control software is mainly consists of an initialization main program and control module flowcharts. The former is performed only once at the beginning, the latter is based on a waiting loop interrupted by the PWM underflow event. The role of the initialization main program is to initialize the system and variable, set and enable the interrupt, then wait for interrupt. Initialization system mainly sets the initial values of the system clock, the watch dog, the event manager, A/D interrupt, and carries on the corresponding set. Variable initialization in the main control algorithm sets the initial value of each variable.

After the system initialization and variable initializations, the software jumps to the waiting loop. It is interrupted every time an interrupt occurs to start the control. The role of the A/D interrupt program is to complete all of the control algorithm. Control system achieve different functions in different periods, this article set selection function module in the A/D interrupt program.

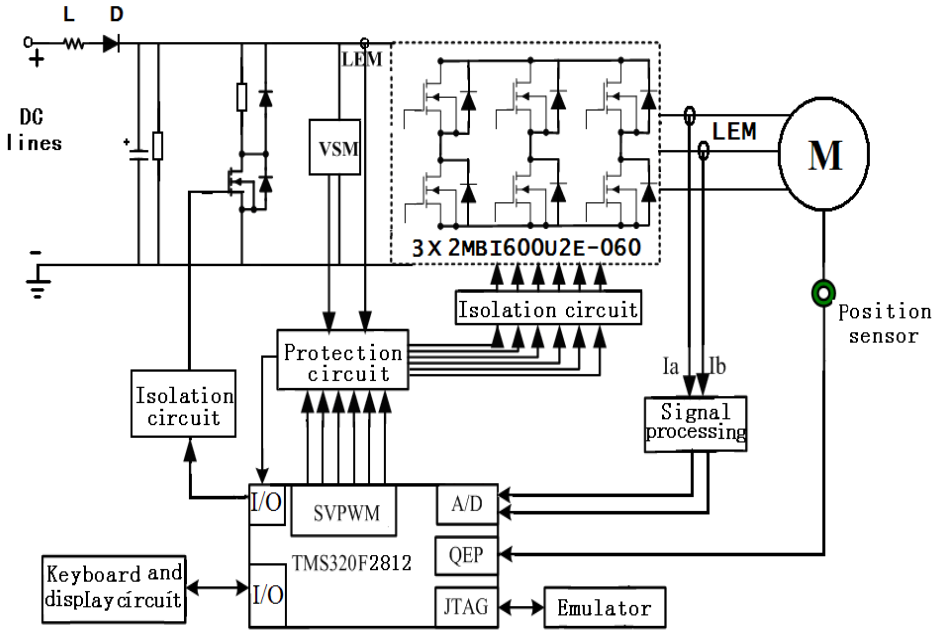

Fig. 9. Principle chart of hardware circuit.

5.3. The System Physical Prototype

Test prototype is shown in Fig. 10. The SPMSM is a 1KW experimental motor. The waveforms are shown in Fig. 11 and Fig. 12. Fig. 11 is estimated position waveforms in zero speed when initial position of the SPMSM is 1 rad. Fig. 12 is estimated position in low speed of 60 rpm under 1rad of initial position. Analysis of test results shows that, SVPWM modulation wave were right, three-phase sinusoidal output current waveform is good, the low harmonic content, the speed of the motor can be fast tracked for a given value, the adjust time is short.

Experimental results show that the proposed algorithm estimates the rotor position well in zero and low speed region. The system has better static, the effectiveness and dynamic performance of the adaptive test signals in a sensorless controlled SPMSM.

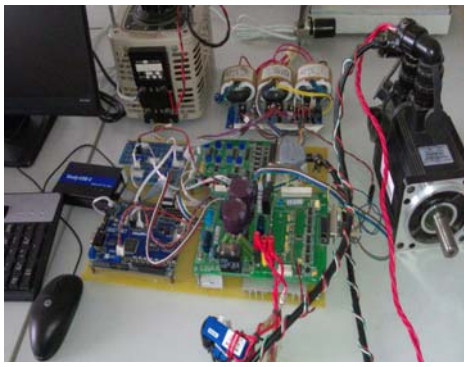

Fig. 10. Test prototype of the system.

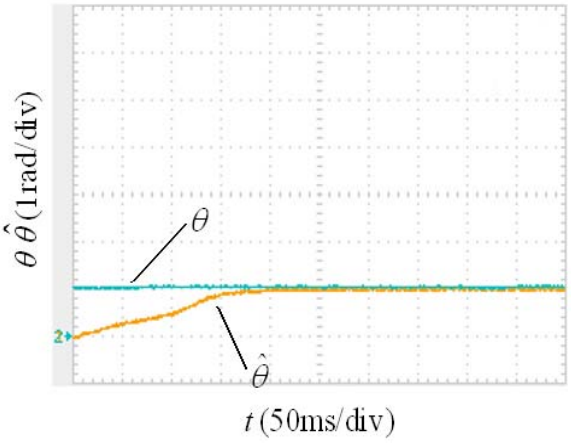

Fig. 11. Estimated position in zero speed.

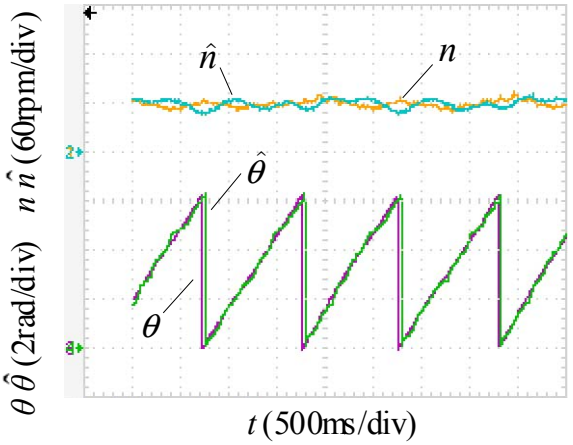

Fig. 12. Estimated position in low speed.

6. Conclusion

This paper presented a sensorless vector control scheme for a SPMSM drive based on the TI TMS320F2812 DSP Controller. It has been shown how the real-time processing capabilities of this DSP controller can lead to a highly reliable and effective drive. Driving reliability, cost effectiveness and efficiency of the system have been improved.

This paper also described the speed variation capability, TMS320F2812 and power electronics hardware, and excellent dynamic behavior. The device has the function of power lost maintain and speed tracking. When DC bus power sudden fails, the electric locomotive speed reduced to a certain speed, the locomotive in the inertia runs, at this point, realizes electric braking. When DC bus power back to normal, the inverter output frequency which is the same to the motor speed, realizes speed tracking.

From results, the output waveforms meet the motor steady operation when input DC bus voltage range from 160 V to 340 V. The device has test run for a year in Coal Industry Group, whose static and dynamic performance is good, to fully meet the requirements of the mining electric locomotive speed. It is proved that the design of the system is validity and feasibility.

Acknowledgements

The paper is supported by Key Open Lab of Control Engineering of Henan Province (Grant No. KG 2011-13), Education Department of Henan Natural Science Research Key Project of China (Grant No.13A470342) and Science and Technology Research Project of China National Coal Association (Grant No. MTKJ2012-369).

References

[1]. Li Zhenbi, Shi Xiaoyan, DC chopped wave speed regulating system of battery locomotive based on DSP control, *Colliery Mechanical & Electrical Technology*, Vol. 2, Issue 1, 2007, pp. 26-28.

[2]. K. W. Lee, D. H. Jung, I. J. Ha, An online identification method for both stator resistance and back-EMF coefficient of PMSM without rotational transducers, *IEEE Transaction on Industry Electronics*, Vol. 51, Issue 3, 2004, pp. 507–510.

[3]. A. Piippo, M. Hinkkanen, J. Luomi, Analysis of an adaptive observer for sensorless control of interior permanent magnet synchronous motors, *IEEE Transaction on Industry Electronic*, Vol. 55, Issue 10, 2010, pp. 570–576.

[4]. M. Eskola and H. Tuusa, Comparison of MRAS and novel simple method for position estimation in PMSM drives, in *Proceedings of the IEEE Power Electronics Specialists Conference PESC*, Acapulco, Mexico, 12-14 June 2003, pp. 550–555.

[5]. Deng Qingyu, Liao Xiaozhong, Dong Lei, A flux observation model of induction motor based on stator flux oriented vector control, *Transactions of China Electrotechnology Society*, Vol. 22, Issue 5, 2007, pp. 30–34.

[6]. Gheorghe Daniel Andreescu, Cristian Ilie Pitic, Combined flux observer with signal injection enhancement for wide speed range sensorless direct torque control of IPMSM drives, *IEEE Transactions on Energy Conversion*, Vol. 23, Issue 1, 2008, pp. 393-402.

[7]. K. W. Lee, D. H. Jung, I. J. Ha, An online identification method for both stator resistance and back-EMF coefficient of PMSM without rotational transducers, *IEEE Transaction on Industry Electronics*, Vol. 51, Issue 8, 2009, pp. 507–510.

[8]. Z. Wang, K. Lu, and F. Blaabjerg, A simple startup strategy based on current regulation for back-EMF based sensorless control of PMSM, *IEEE Transactions on Power Electronics*, Vol. 27, Issue 8, 2012, pp. 3817–3825.

[9]. T. F. Chan, W. Wang, P. Borsje, Y. K. Wong, Sensorless permanent-magnet synchronous motor drive using a reduced-order rotor flux observer, *IET Electric Power Applications*, Vol. 2, Issue 2, 2008, pp. 88–98.

[10]. Li Shuai, Zhou Bo, Liu Ying, Feng Ying, A novel method of initial rotor position estimation for surface mounted permanent magnet synchronous motor, in *Proceedings of the IEEE Conference on Electrical*

and Control Engineering (ICECE '2010), Wuhan, China, 16-19 June 2010, pp. 4924-4927.
[11]. Mohammad Ali, Ghazi Moghadam, Farzad Tahami, Sensorless control of PMSMs with tolerance for delays and stator resistance uncertainties, *IEEE Transactions on Power Electronics*, Vol. 28, Issue 3, 2013, pp. 1391-1399.
[12]. Frederik M. L. De Belie, Jan A. Melkebeek, A sensorless drive by applying the average-current samples, *IEEE Transactions on Power Electronics*, Vol. 25, Issue 7, 2010, pp. 875–887.
[13]. M. Hinkkanen, T. Tuovinen, L. Harnefors, and J. Luomi, A combined position and stator-resistance observer for salient PMSM drives: design and stability analysis, *IEEE Transactions on Power Electronics*, Vol. 27, Issue 10, 2012, pp. 601–609.
[14]. Frederik M. L. De Belie, Peter Sergeant, Jan A. Melkebeek, A sensorless drive by applying the average-current samples, *IEEE Transactions on Power Electronics*, Vol. 25, Issue 7, 2010, pp. 875–887.
[15]. G. Adamidis, Z. Koutsogiannis, and P. Vagdatis, Investigation of the performance of a variable-speed drive using direct torque control with space vector modulation, *Proceedings on Electric Power Components and Systems*, Vol. 39, Issue 7, 2011, pp. 1227–1243.
[16]. S. C. Yang and R. D. Lorenz, Surface permanent magnet synchronous machine position estimation at low speed using eddy current reflected asymmetric resistance, *IEEE Transactions on Power Electronics*, Vol. 27, Issue 7, 2012, pp. 2595–2604.
[17]. Prasanta Sarkar, Sagarika Pal, Swadhin Sambit Das, Identification and speed control of PMDC motor using time moments, *Sensors & Transducers*, Vol. 119, Issue 8, August 2010, pp. 151-161.
[18]. Prasanta Sarkar, Sagarika Pal, Swadhin Sambit Das, Parameter estimation and speed control of PMDC servo motor using method of time moments, *Sensors & Transducers*, Vol. 119, Issue 8, August 2010, pp. 162-173.